

Polar interface vibrations in GaN/AlN quantum dots: Essential effects of crystal anisotropy

D. A. Romanov and V. V. Mitin

Department of Electrical & Computer Engineering, Wayne State University, Detroit, Michigan 48202

M. A. Stroschio*

US Army Research Office, P.O. Box 12211, Research Triangle Park, North Carolina 27695-7911

(Received 21 December 2001; revised manuscript received 10 May 2002; published 26 September 2002)

The inherent anisotropy of crystal lattices of the nitride semiconductor compounds is found to essentially determine the character of surface polar vibrations of a GaN quantum dot in AlN matrix. The interface phonons are analyzed within the framework of the anisotropic macroscopic dielectric continuum model. Analytical solutions are obtained for surface modes on a quantum dot of oblate spheroidal form. These modes can exist in continuous frequency regions, in contrast to quantized frequencies that are characteristic for isotropic case. The period of spatial oscillations in these modes varies substantially over the dot surface, so that the oscillations can have condensation points at the dot poles. Along with truly localized surface states, there are two other types of phonon modes. First, runaway modes, which freely leave the dot surface through escape roots in equatorial regions. Second, quasistationary (leaky) states, in which the areas of spatial oscillations are separated from the escape root regions by the areas of exponential behavior. The leaky states can provide effective energy relaxation of the confined electrons.

DOI: 10.1103/PhysRevB.66.115321

PACS number(s): 63.22.+m, 63.20.Kr

I. INTRODUCTION

Wide-band-gap nitride semiconductor materials are of substantial current interest in view of their potential applications in electronics, optoelectronics, biomedical physics, etc. (see Ref. 1). Besides their conspicuous advantages in these fields, quantum structures based on nitride semiconductors are quite attractive from a purely physical standpoint; their fundamental physical properties can be affected and even determined by the interplay of spatial quantization and inherent anisotropy of the crystal structure.

Both GaN and AlN usually crystallize in the hexagonal wurtzite structure of space group C_{6v}^4 . These wurtzites are uniaxial crystals with the optical axis coinciding with the c axis of the crystal structure that is perpendicular to the hexagons. Due to this uniaxial anisotropy, in bulk crystals the optical phonons are classified into the so-called ordinary and extraordinary modes. The frequencies of the latter depend essentially on the angle between the phonon wave vector and the c axis. In Ref. 2, the authors investigated polar optical phonons in GaN/AlN quantum well (perpendicular to the c axis) in the framework of the macroscopic dielectric continuum model,³ modified for the uniaxial case. They found a number of essential distinctions from the well-studied case of the conventional GaAs/AlAs structure.⁴ Most notably, the confined phonon modes demonstrated substantial tails in the barrier media and acquired finite dispersion. Also, it was shown that though interface modes at a single heterointerface are dispersionless and correspond to a few distinct frequencies, as was the case in GaAs/AlAs structure,⁴ proper choice of the material composition in $\text{Ga}_x\text{Al}_{1-x}\text{N}/\text{AlN}$ structure can eliminate some of these interface modes.

Given this precursor, it is interesting and instructive to study the polar phonon modes in a quantum dot in the GaN/AlN system. In this case, the local orientation of the interface with respect to the c axis will vary over the dot, which can

well invoke yet new features of the phonon spectrum. In this investigation, it is natural to refer to the known case of optical phonons in zinc-blende GaAs/AlAs structures. Quantum dots in these structures have been studied by many authors (see Refs. 5–9 and references therein) in the framework of different models. In particular, in the above-mentioned dielectric continuum model, the interface phonon spectra were found for spherical and spheroidal dots.^{5,6,9} In these cases, each of the allowed frequencies of the planar single heterointerface⁴ is split into a convergent series of distinct frequencies labeled by the angular quantum number, in the case of a spherical dot, or by angular and magnetic quantum numbers, in the case of a spheroidal dot.

In the present paper, we will use the dielectric continuum model to consider surface polar vibrations of a GaN quantum dot in an AlN matrix. We will show that the anisotropy considerably enhances the variety of possible polar vibrations. In contrast to a series of distinct localized modes of an isotropic GaAs dot, in the GaN dot allowed frequency windows emerge, along with specific leaky and runaway states which can play an important role in the processes of electron energy relaxation.

The paper is organized as follows. In Sec. II, we briefly describe the dielectric continuum approach, introduce the dimensionless material parameters, give the basic equations in curvilinear coordinates, and transform the dielectric permittivity tensor to spheroidal coordinates, thus obtaining the system of equations describing the optical phonon modes near the quantum dot. In Sec. III, we reduce the problem to surface modes and obtain a formal analytical solution for these modes. In Sec. IV, we numerically analyze the physical conditions for the existence of the surface modes, obtain the regions of existence for the stationary and quasistationary surface modes, and discuss the peculiar character of these modes. Finally, in Sec. V, we summarize the results obtained and briefly mention their possible significance for the elec-

TABLE I. Characteristic phonon parameters of GaN/AlN system.

	ε_∞	$\omega_{L\tau}$	ω_{Ll}	$\omega_{T\tau}$	ω_{Tl}
GaN	5.29	1.39	1.38	1.05	1
AlN	4.68	1.72	1.68	1.26	1.24

tron energy relaxation in the dot.

II. BASIC EQUATIONS

In the adopted macroscopic dielectric continuum model, neglecting the retardation effects, the phonon-borne part of the polarization in the two media labeled by index i ($i=1$ stays for GaN and $i=2$ for AlN) is determined entirely by the equation for the electric potential, $\psi^{(i)}(\omega, \mathbf{r})$:

$$\text{div}[\hat{\varepsilon}^{(i)}(\omega)\text{grad}(\psi^{(i)}(\omega, \mathbf{r}))]=0. \quad (1)$$

Here, $\hat{\varepsilon}^{(i)}(\omega)$ is the frequency-dependent dielectric permittivity tensor that, reflects uniaxial anisotropy of the crystal structure. In the Cartesian coordinates with the z axis coinciding with the crystallographic c axis of the wurtzite structure, this tensor has the diagonal form

$$\hat{\varepsilon}^{(i)}(\omega) = \begin{pmatrix} \varepsilon_\tau^{(i)}(\omega) & 0 & 0 \\ 0 & \varepsilon_\tau^{(i)}(\omega) & 0 \\ 0 & 0 & \varepsilon_l^{(i)}(\omega) \end{pmatrix}, \quad (2)$$

with the components

$$\varepsilon_l^{(i)}(\omega) = \varepsilon_\infty^{(i)} \frac{\omega^2 - (\omega_{Ll}^{(i)})^2}{\omega^2 - (\omega_{Tl}^{(i)})^2}, \quad \varepsilon_\tau^{(i)}(\omega) = \varepsilon_\infty^{(i)} \frac{\omega^2 - (\omega_{L\tau}^{(i)})^2}{\omega^2 - (\omega_{T\tau}^{(i)})^2}. \quad (3)$$

In these expressions, we assume that the high-frequency dielectric susceptibilities $\varepsilon_\infty^{(i)}$ are isotropic in both media. Thus, the anisotropic dielectric properties of the two media are determined by the characteristic frequencies of the longitudinal-optical phonons ($\omega_{Ll}^{(i)}$ for the phonon propagating along the z axis and $\omega_{L\tau}^{(i)}$ for the phonon propagating in the x - y plane) and the transverse-optical phonons ($\omega_{Tl}^{(i)}$ and $\omega_{T\tau}^{(i)}$, respectively). In what follows, we use the lowest of these frequencies, that of the Tl phonon in GaN, $\omega_{Tl}^{(1)}$ as the frequency unit. The values of $\varepsilon_\infty^{(i)}$, along with the eight characteristic frequencies normalized to $\omega_{Tl}^{(1)}$ are given in Table I.

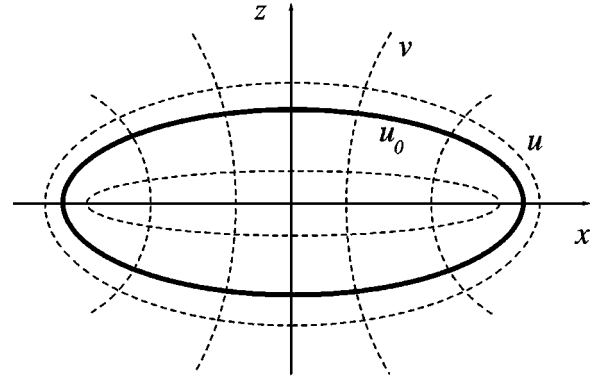
In addition to Eq. (1), the electric potential should satisfy boundary conditions on the interface of the two media:

$$\psi^{(1)}(\omega, \mathbf{r}_s) = \psi^{(2)}(\omega, \mathbf{r}_s) \quad (4)$$

and

$$[\mathbf{n}(\mathbf{r}) \cdot \text{grad}(\psi^{(1)}(\omega, \mathbf{r}))]|_{\mathbf{r}=\mathbf{r}_s} = [\mathbf{n}(\mathbf{r}) \cdot \text{grad}(\psi^{(2)}(\omega, \mathbf{r}))]|_{\mathbf{r}=\mathbf{r}_s}. \quad (5)$$

In these equations, \mathbf{r}_s is the position vector of a point at the interface, and $\mathbf{n}(\mathbf{r}_s)$ is a unit normal vector at this point (directed from medium 1 to medium 2).



$$\begin{aligned} z &= a \sinh u \cos v \\ y &= a \cosh u \sin v \sin \phi \\ x &= a \cosh u \sin v \cos \phi \end{aligned}$$

FIG. 1. The dot as an oblate spheroid, with the related spheroidal coordinate system. The crystal c axis is along the z axis; the dot surface corresponds to $u = u_0 = \text{const}$; the points at this surface are indicated by the coordinates v and ϕ .

Since in anisotropic media, the spherical shape has no advantages of simplicity, we model the quantum dot as an oblate spheroid with the rotational axis directed along the crystallographic c axis of AlN and GaN. Accordingly, we use the oblate spheroidal coordinates¹⁰ see (Fig. 1):

$$\begin{aligned} x &= a \cosh u \sin v \cos \phi, \\ y &= a \cosh u \sin v \sin \phi, \end{aligned} \quad (6)$$

$$z = a \sinh u \cos v.$$

The surfaces $u = \text{const}$ are oblate spheroids; the dot surface corresponds to a certain value, $u = u_0$. The surfaces $v = \text{const}$ are one-sheet hyperboloids of revolution. The value of the parameter u_0 determines the spheroid flatness: when $u_0 \rightarrow 0$, the spheroid degenerates into a disk; and when $u \rightarrow \infty$, the spheroid becomes a sphere, provided $a \cosh u = \text{const} = R$, the sphere radius.

Applying the coordinate transformation of Eq. (6) to the dielectric permittivity tensor of Eq. (2), we obtain, after some algebra, the dielectric permittivity tensor in the oblate spheroidal coordinates:

$$\hat{\varepsilon}^{(i)}(\omega, u, v) = \begin{pmatrix} \varepsilon_1^{(i)}(\omega, u, v) & \varepsilon_2^{(i)}(\omega, u, v) & 0 \\ \varepsilon_2^{(i)}(\omega, u, v) & \varepsilon_1^{(i)}(\omega, u, v) & 0 \\ 0 & 0 & \varepsilon_\tau^{(i)}(\omega) \end{pmatrix}, \quad (7)$$

where

$$\varepsilon_1^{(i)}(\omega, u, v) = \frac{\varepsilon_\tau^{(i)}(\omega) \sinh^2 u \sin^2 v + \varepsilon_l^{(i)}(\omega) \cosh^2 u \cos^2 v}{\sinh^2 u + \cos^2 v}$$

$$\varepsilon_2^{(i)}(\omega, u, v) = \frac{(\varepsilon_\tau^{(i)}(\omega) - \varepsilon_l^{(i)}(\omega)) \sinh u \cosh u \sin v \cos v}{\sinh^2 u + \cos^2 v}. \quad (8)$$

Thus, in the oblate spheroidal coordinates the dielectric permittivity tensor becomes nondiagonal and position dependent. Note that the off-diagonal elements are proportional to $[\varepsilon_\tau^{(i)}(\omega) - \varepsilon_l^{(i)}(\omega)]$, and thus owe their existence to the anisotropy of the media. Moreover, the position dependence is also caused by the anisotropy; if $\varepsilon_\tau^{(i)}(\omega) = \varepsilon_l^{(i)}(\omega) = \varepsilon^{(i)}(\omega)$, the tensor of Eq. (7), as well as the tensor of Eq. (2), duly degenerates into the scalar $\varepsilon^{(i)}(\omega)$.

The nondiagonality of the permittivity tensor means that the variables in Eq. (1) [and in the boundary conditions (4) and (5)] are no longer separable. This, in turn, means that the solution cannot be found in a general form. We restrict ourselves to considering only interface vibrations well localized near the dot surface.

III. ANALYTICAL SOLUTION

To obtain the interface modes, we present the electric potential inside the dot, $\psi^{(1)}(\omega, \mathbf{r})$, and outside the dot, $\psi^{(2)}(\omega, \mathbf{r})$, in the approximate close-to-surface form,

$$\psi^{(i)}(\omega, u, v, \varphi) = e^{im\varphi} e^{\kappa^{(i)}(\omega, u_0)(u - u_0)} \chi(\omega, u_0, v). \quad (9)$$

Here, m is the rotational quantum number and $\kappa^{(1)}$ and $\kappa^{(2)}$ are the dimensionless inverse localization lengths. We assume these lengths to be sufficiently small, so that

$$\kappa^{(1)}, \kappa^{(2)} \gg 1. \quad (10)$$

Substitution of this form of the potential in Eqs. (1), (4), and (5) gives us the system of three differential equations for $\kappa^{(1)}$, $\kappa^{(2)}$, and χ as functions of variable v :

$$\frac{d^2 \chi}{dv^2} + 2 \frac{f_2^{(1)}}{f_2^{(1)}} \kappa^{(1)} \frac{d\chi}{dv} + \left[(\kappa^{(1)})^2 - \frac{\varepsilon_\tau^{(1)} m^2}{f_0^2 f_1^{(1)}} \right] \chi = 0,$$

$$\frac{d^2 \chi}{dv^2} + 2 \frac{f_2^{(2)}}{f_2^{(2)}} \kappa^{(2)} \frac{d\chi}{dv} + \left[(\kappa^{(2)})^2 - \frac{\varepsilon_\tau^{(2)} m^2}{f_0^2 f_1^{(2)}} \right] \chi = 0, \quad (11)$$

$$f_1^{(1)} \kappa^{(1)} \chi + f_2^{(1)} \frac{d\chi}{dv} = f_1^{(2)} \kappa^{(2)} \chi + f_2^{(2)} \frac{d\chi}{dv}.$$

Here, the auxiliary functions are

$$f_0(u_0, v) = \frac{\cosh u_0 \sin v}{\sinh^2 u_0 + \cos^2 v}, \quad (12)$$

$$f_1^{(i)}(\omega, u_0, v) = \varepsilon_\tau^{(i)}(\omega) \sinh^2 u_0 \sin^2 v + \varepsilon_l^{(i)}(\omega) \cosh^2 u_0 \cos^2 v, \quad (13)$$

$$f_2^{(i)}(\omega, u_0, v) = \frac{1}{4} [\varepsilon_\tau^{(i)}(\omega) - \varepsilon_l^{(i)}(\omega)] \sinh(2u_0) \sin(2v). \quad (14)$$

The first two of Eqs. (11) originate from Eq. (1), the third equation originates from the boundary condition (5).

The fact that the third equation in Eq. (11) contains first derivative with respect to v allows us to find formal analytical solution of the system (11), under the assumption of Eq. (10). The localization lengths are found to be

$$\kappa^{(i)} = \frac{|m|}{f_0 f_1^{(i)}} \left((-1)^k f_2^{(i)} \sqrt{\frac{\varepsilon_\tau^{(1)} f_1^{(1)} - \varepsilon_\tau^{(2)} f_1^{(2)}}{F^{(1)} - F^{(2)}}} + (-1)^n \sqrt{\frac{\varepsilon_\tau^{(2)} f_1^{(2)} F^{(1)} - \varepsilon_\tau^{(1)} f_1^{(1)} F^{(2)}}{F^{(1)} - F^{(2)}}} \right), \quad (15)$$

where

$$F^{(i)} = (f_1^{(i)})^2 - (f_2^{(i)})^2, \quad (16)$$

$k=0,1$ and $n=0,1$.

The function $\chi(\omega, u_0, v)$ is determined by the expression

$$\frac{d}{dv} (\ln \chi) = (-1)^{k+1} \frac{|m|}{f_0} \sqrt{\frac{\varepsilon_\tau^{(1)} f_1^{(1)} - \varepsilon_\tau^{(2)} f_1^{(2)}}{F^{(1)} - F^{(2)}}}. \quad (17)$$

Note that the radical in Eq. (17) is the same as the first radical in Eq. (15). Note also that the pseudo-WKB form of the function $\chi(\omega, u_0, v)$ in Eq. (17) results from the previously mentioned assumption and requires, at least, nonzero value of the angular quantum number m . Various choices of the integer numbers k and n in formulas (15) and (17) give four independent formal solutions. However, not all these solutions are physically possible at given values of the variables ω and v . Their number is significantly restricted by the physical requirements that we consider in the following section.

IV. CLASSIFICATION OF THE SURFACE VIBRATIONS

Depending on the parameters involved, not all of the four independent solutions obtained in Sec. III are always feasible. Specifically, to describe interface states, the localization parameters $\kappa^{(1)}$ and $\kappa^{(2)}$ should provide evanescent dependence of $\psi^{(1)}$ and $\psi^{(2)}$ on $|u - u_0|$. Since each radical in formula (15) can have either real or imaginary value, depending on ω and v , this requirement leads to the condition

$$\text{Re}(\kappa^{(1)}) \text{Re}(\kappa^{(2)}) < 0. \quad (18)$$

Since the inverse localization lengths $\kappa^{(1)}$ and $\kappa^{(2)}$ are complex functions of the frequency ω and the coordinate v , the condition of Eq. (18) determines the allowed windows for the surface states in the (ω, v) plane. Within these windows, the character of the surface vibrations is determined by the sign of the expression under the radical in formula (17); negative sign corresponds to spatial oscillations; positive sign corresponds to evanescent or growing "under barrier" exponentials. We present typical (ω, v) charts (for $u_0 = 1$ and

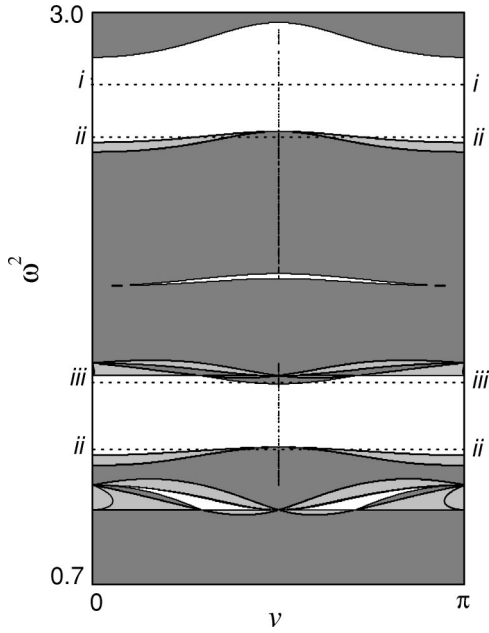


FIG. 2. The polar vibrations chart for $u_0=1.0$. The white areas are the windows of spatial oscillations; the shadowed areas are the escape regions; and the dark areas are the areas of exponential behavior. The three types of interface states are indicated in (a) by dashed lines, *i* represents localized states, *ii* represents leaky states, and *iii* represents runaway states.

($u_0=0.1$) in Figs. 2 and 3. In these figures, the areas of spatial oscillations are white and denoted as I, the areas of surface-state nonexistence (phonon escape) are shadowed and denoted as II, and the underbarrier areas are dark and denoted as III. As it is seen, while the dot form changes from disklike ($u_0=0.1$) to almost spherical ($u_0=1$), the form of these areas evolve substantially. However, the main features of the

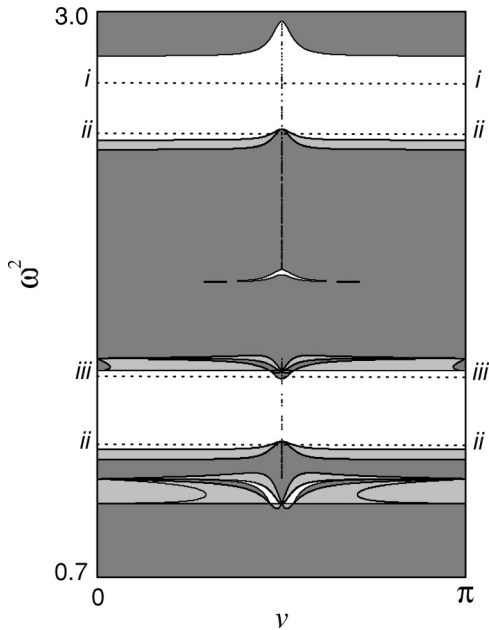
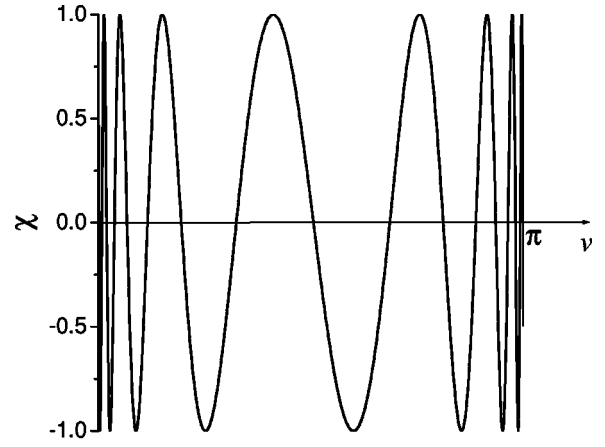


FIG. 3. The polar vibrations chart for $u_0=0.1$. Notation is the same as in Fig. 2.



$$u_0=1; m=7; \omega^2=2.6$$

FIG. 4. The function $\chi(\nu)$ for a localized interface state in the middle of an allowed frequency strip. Note the “chirping” form of the function, with the condensation points at the dot poles, $\nu=0$ and $\nu=\pi$.

chart persist; at a given frequency, the anisotropy pushes the surface states towards the dot poles while the equatorial regions correspond to the escape routes. Also, it can be mentioned that, in contrast to the areas of types I and II, the areas of type III never go uninterrupted throughout the whole range of the ν variable. Typically, the areas of type III lie between areas of type I and areas of type II; they never have the areas of the same type on both borders.

A. Oscillatory behavior

Here, we describe in more detail the peculiar character of the previously derived interface states. In the type-I areas of the (ω, ν) plane, where the argument of the radical in formula (17) is negative, the integration yields complex exponentials. It is convenient to combine them into even and odd functions and write these functions as follows. For the even states,

$$\chi_e(\nu) = \cos \left(|m| \int_{\pi/2 f_0(\nu')}^{\nu} \frac{d\nu'}{\pi/2 f_0(\nu')} \sqrt{\frac{\varepsilon_\tau^{(2)} f_1^{(2)}(\nu') - \varepsilon_\tau^{(1)} f_1^{(1)}(\nu')}{F^{(1)}(\nu') - F^{(2)}(\nu')}} \right); \quad (19)$$

for the odd states,

$$\chi_o(\nu) = \sin \left(|m| \int_{\pi/2 f_0(\nu')}^{\nu} \frac{d\nu'}{\pi/2 f_0(\nu')} \sqrt{\frac{\varepsilon_\tau^{(2)} f_1^{(2)}(\nu') - \varepsilon_\tau^{(1)} f_1^{(1)}(\nu')}{F^{(1)}(\nu') - F^{(2)}(\nu')}} \right). \quad (20)$$

For small values of ν , $f_0 \propto \nu$. This causes the integrals in formulas (19) and (20) to diverge logarithmically when $\nu \rightarrow 0$, unless the expression under the radical also goes to zero, which happens only at the borders of the allowed windows. Thus, in general, near the point $\nu=0$, the argument of the trigonometric functions in Eqs. (19) and (20) behaves as $\ln(\nu)$ and causes functions $\chi_e(\nu)$ and $\chi_o(\nu)$ to oscillate rapidly when ν approaches zero (see Fig. 4). These rapid oscil-

lations might seem to create nonphysical divergence in the electric-field magnitude and the atomic displacement amplitudes. However, the localization lengths of Eq. (15) shrink to zero in this same region. This circumstance effectively eliminates the divergence. It should be noted also that when the oscillations of $\chi(v)$ become essentially of short wavelength, they cannot be treated within the model employed.

B. Exponential behavior

In the type-III areas of the (ω, v) plane, where the argument of the radical in formula (17) is positive, the formula yields

$$\begin{aligned} \chi(v) = & A \exp\left(|m| \int_{\pi/2}^v \frac{dv'}{f_0(v')}\right) \\ & \times \sqrt{\frac{\varepsilon_\tau^{(2)} f_1^{(2)}(v') - \varepsilon_\tau^{(1)} f_1^{(1)}(v')}{F^{(1)}(v') - F^{(2)}(v')}} \\ & + B \exp\left(-|m| \int_{\pi/2}^v \frac{dv'}{\pi/2 f_0(v')}\right) \\ & \times \sqrt{\frac{\varepsilon_\tau^{(2)} f_1^{(2)}(v') - \varepsilon_\tau^{(1)} f_1^{(1)}(v')}{F^{(1)}(v') - F^{(2)}(v')}}. \end{aligned} \quad (21)$$

where the constants A and B are determined by matching on the area boundary.

As was already mentioned, the areas of type III do not go uninterrupted throughout the whole range of v . Thus, at a given ω , the segment of validity of Eq. (21) either reaches the dot pole on one side and borders an escape region on the other side, or borders an oscillatory region on one side and an escape region on the other side. If the extension to the pole is the case, the integrals in Eq. (21) diverge logarithmically, just as in Eqs. (19) and (20). In this case, we need to take $B=0$ to avoid divergence of the function $\chi(v)$ itself. Thus, when $v \rightarrow 0$, the function $\chi(v)$ behaves as $v^{|m|}$. When v grows, the function $\chi(v)$ also grows monotonically up to the boundary of the area. The exception of this generic behavior is the case when the expression under the radical is zero at the point $v=0$. This corresponds to the boundary of a type-III area in the (ω, v) plane. In this case, the choice $A=0$ in formula (21) is also allowed. Then, the formula describes a function that is concentrated near the pole and rapidly decreases away from it.

In the case when the area of type III is sandwiched between an area of type I and an area of type II, both choices of $A=0$ and $B=0$ in formula (21) are possible. The first choice corresponds to a function decreasing from the escape route, i.e., a penetrating state. The second choice corresponds to a function decreasing from the oscillatory region to the escape route, i.e., a quasistationary state. In the latter case, the ratio of the amplitudes of the function χ at the I-III boundary and at the III-II boundary gives the lifetime of this state.

The character of the exponential states is illustrated in Fig. 5. Here, we take the frequency corresponding to the upper edge of the upper dark area in Fig. 2 at $v=0$. The

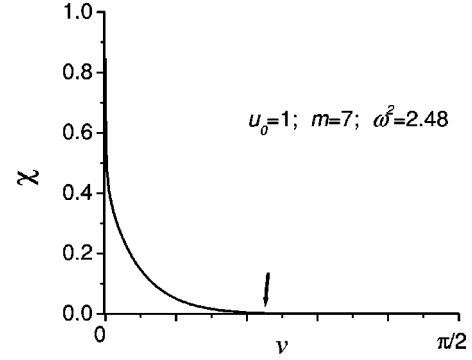


FIG. 5. The function $\chi(v)$ in the region of exponential behavior. The frequency is taken of the top edge of the top dark area in Fig. 2. The function drops at the onset of the escape region.

argument of the radicals in Eq. (21) being zero at $v=0$ allows us to choose $A=0$, i.e., a quasistationary state around the pole. As seen in Fig. 5, the lifetime of this state can be estimated as $10^{-4}/\omega$.

To summarize this analysis and classification, the surface phonon modes can generally fall into three categories: (i) truly localized modes, which sustain oscillatory character throughout the dot surface (these modes are marked i in Fig. 2), (ii) quasistationary, or leaky, modes; for which the regions of spatial oscillations are surrounded by barrier regions followed by regions of the surface-state nonexistence, i.e., escape routes (these modes are marked ii in Fig. 2), (iii) runaway modes, for which the regions of surface-state nonexistence directly neighbor the previously mentioned oscillatory regions (these modes are marked iii in Fig. 2).

The escape routes for quasistationary modes and for runaway modes lie in the equatorial region of the dot. The lifetimes of quasistationary modes depend essentially on the value of u_0 , i.e., on the aspect ratio of the dot spheroid.

V. CONCLUSIONS

We have analyzed polar vibrations of a GaN/AlN quantum dot in the framework of the anisotropic macroscopic dielectric continuum model, and obtained formal analytical solutions for interface modes on a quantum dot of oblate spheroidal form. The crystal anisotropy makes these modes drastically different from their analogs in spherical^{5,6,8} and even spheroidal^{6,9} quantum dots in the GaAs/AlAs system. Specifically, the allowed modes exist in continuous allowed frequency windows rather than at discrete frequencies. Moreover, the spatial oscillations of these modes can have condensation points at the dot poles.

Qualitatively, this striking difference from the case of cubic semiconductors can be understood by comparing interface modes for a plane boundary of two isotropic media⁴ and interface modes for a plane (0001) boundary of two media of wurtzite symmetry.² In the former case, there exist just two singular frequencies of the interface mode; in the latter case, the anisotropy of the wurtzite structure leads to dispersion of these energy levels. On the other hand, in isotropic media, for a spherical dot, both of the singular energy levels split into convergent series labeled by the angular quantum num-

ber; for spheroidal dot, additional splitting by the magnetic quantum number occurs. Then, it is not unnatural that in a wurtzite spheroidal dot, the combination of these two effects, dispersion and splitting, results in the allowed frequency windows.

In addition to the truly localized surface states of the allowed frequency windows, there always exist runaway modes that freely leave the dot surface through escape roots in equatorial regions. There also exist quasistationary (leaky) states, in which the areas of spatial oscillations are separated from the escape route regions by the areas of exponential behavior.

To the best of our knowledge, no direct experimental evidence has verified these results so far. However, Raman-scattering results provide indirect evidence. In particular, we cite recent Raman-scattering experiments in GaN/AlN quantum dot systems.¹¹ In these experiments, Raman peaks were observed at room temperature, and redshift of these peaks with respect to the phonon frequencies in bulk GaN and AlN was indicated. The authors ascribe the redshift to the strain fields, though some features, including inhomogeneous broadening of the peaks, remain unexplained. Since the two

allowed frequency windows in Fig. 2 lie below the respective frequencies of longitudinal phonons, the observed redshift can be caused by the localized phonon states we describe here, or the combination of the localization and the strain. The role of the allowed frequency window surface states can be confirmed if the peaks remain broadened at lower temperatures. Another indication of the surface states can be weak transitions involving *c*-axis polarization.

Finally, the broadband character of the interface states is likely to facilitate energy relaxation of electrons confined in the dot; the continuous regions of allowed phonon energy can make it easy to match the electron energies in multiphonon processes, while the leaky states can provide effective energy removal from the dot surface. Quantitative discussion of these effects requires proper description of electron quantization in a wurtzite dot and lies well beyond the scope of this paper.

ACKNOWLEDGMENT

This work was supported by the US Army Research Office through Contract No. DAAH04-96-C-0086.

*Present address: Electrical and Computer Engineering and Bioengineering Departments, University of Illinois at Chicago, Chicago, IL 60607.

¹S. Nakamura and G. Fasol, *The Blue Laser Diode* (Springer-Verlag, Berlin, 1997).

²B.C. Lee, K.W. Kim, M.A. Stroscio, and M. Dutta, *Phys. Rev. B* **58**, 4860 (1998); S.M. Komirenko, K.W. Kim, M.A. Stroscio, and M. Dutta, *ibid.* **59**, 5013 (1999).

³M. Cardona, in *Lectures on Surface Science*, edited by G. R. Castro and M. Cardona (Springer-Verlag, Berlin, 1987).

⁴N. Mori and T. Ando, *Phys. Rev. B* **40**, 6175 (1989).

⁵R.M. de la Cruz, S.W. Teitworth, and M.A. Stroscio, *Phys. Rev. B* **52**, 1489 (1995).

⁶P.A. Knipp and T.L. Reinecke, *Phys. Rev. B* **46**, 10 310 (1992).

⁷S. Nomura and T. Kobayashi, *Phys. Rev. B* **45**, 1305 (1992).

⁸E. Roca, C. Trallero-Giner, and M. Cardona, *Phys. Rev. B* **49**, 13 704 (1994).

⁹F. Comas, C. Trallero-Giner, Nelson Studart, and G.E. Marques, *Phys. Rev. B* **65**, 073303 (2002).

¹⁰G. A. Korn and T. M. Korn, *Mathematical Handbook for Scientists and Engineers*, 2nd ed. (McGraw-Hill, New York, 1968).

¹¹J. Gleize, J. Frandon, F. Demangeot, M.A. Renucci, C. Adelman, B. Daudin, G. Feuillet, B. Damilano, N. Grandjean, and J. Massies, *Appl. Phys. Lett.* **77**, 2174 (2000).